PROCEEDINGS, 48th Workshop on Geothermal Reservoir Engineering
Stanford University, Stanford, California, February 6-8, 2023
SGP-TR-224

Identification of Geothermal Surface Manifestation Using ASTER Satellite Imagery. Case Study: Geothermal systems in Nakuru County, Kenya

Mathew Kamau

mwkamau@kengen.co.ke

Keywords: ASTER, Hydrothermal alteration, geothermal manifestations, processing techniques, band ratios

ABSTRACT

Advancement in spectral resolution, spatial resolution, image processing techniques and the quality of remote sensing satellite imagery have enabled use of satellite data for extensive exploration and characterization of geothermal potential areas. In this research, geothermal alteration minerals and mineral assemblages were studied using ASTER a multispectral instrument at two known geothermal potential areas within Nakuru County. VNIR & SWIR ASTER data was used to characterize hydrothermal altered zones in the study area. Red-Green-Blue (RGB) band combinations, Band ratios, color composite, Relative Absorption Band Depth and Logical Operator Algorithm processing techniques were applied to extract spectral information of important rocks and hydrothermal alteration minerals in the study area. The techniques were used to enhance geological features by contrasting alteration zones and different lithologies occurring in the study area. Zones with high concentrations of argillic, phyllic, propylitic alteration mineral assemblages were enhanced. The study aimed to demonstrate use of satellite imagery in bring down exploration cost by narrowing down to areas that shows geothermal potential. The current study proved ASTER processing techniques to be a valuable mapping tools for geological reconnaissance of a large area thus providing preliminary lithologic and hydrothermal alterations maps that are accurate as well as time and cost effective.

1. INTRODUCTION

Launched by NASA on EOS/Terra platform on 18th December 1999, The Advanced Space -borne Thermal Emission and Reflection Radiometer (ASTER) is a multispectral sensor with 14 bands that can measure reflected and emitted electromagnetic radiation from the Earth's surface (Pour et al, 2011). It was built by Japan's Ministry of Economy Trade and Industry (METI). It is a remote sensing sensor which was conceived as a geologic mapping instrument (Abrams & Yamaguchi, 2019). It consist of three separate instrument sub-systems which provides observation in three different spectral regions of the electromagnetic spectrum (Beiranvand et al, 2012). They include Visible and Near Infrared (VNIR), Shortwave Infrared (SWIR) and Thermal Infrared (TIR). It measures three bands in VNIR (B1-B3) which is useful for detecting iron oxides and vegetation cover, six band (B4-B9) within the SWIR wavelength range which are good for identifying clay minerals with diagnostic absorption features at 2.2 um wavelength range and five bands in TIR (B10-B14) which is capable of mapping quartz, mafic minerals and carbonate rocks (Hewson et al., 2019). Figure 1 is the comparison of sensor capabilities of ASTER sensors with those of Landsat 7 ETM+.

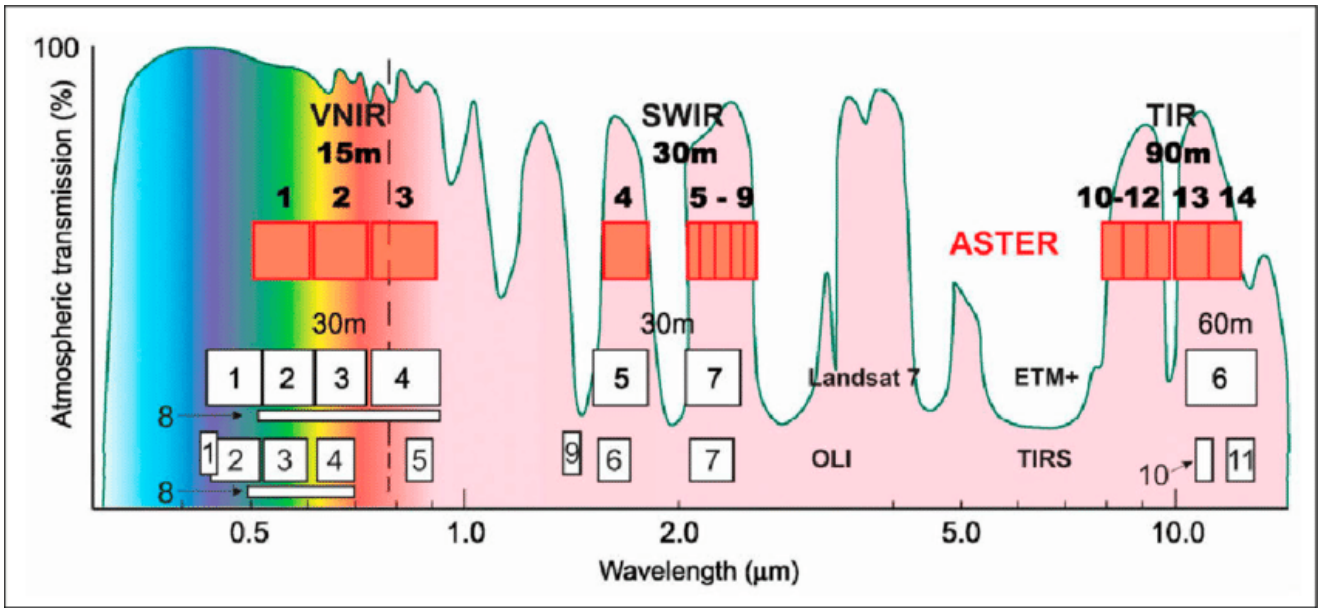

Figure 1: Spectral bands of ASTER and Landsat 7 ETM (Testa et al, 2018)

Previously, ASTER data has been used for mapping hydrothermal alteration minerals both in mineral and geothermal exploration. For instance, Rowan et al, 2003, used ASTER data to map hydrothermal alteration mineral and zones at the cuprite, Nevada test site. Abubakar et al, 2019 used ASTER data for identification of hydrothermal alteration minerals associated with geothermal system in Yankari Park, NE Nigeria. Other studies includes that of Elsaid et al, 2014 who used ASTER data as aid for Uranium exploration in Elmissikat-Eleridiyua granite, Central Eastern Desert, Egypt. Fatima et al, 2017 used ASTER data for mineral identification and mapping in Pakistan and Alimohammadi et al, 2015 for exploration of porphyry copper deposits in the southern part of the Kerman Copper belt, Iran amongst others. Most recently, Hewson et al., 2019 applied ASTER day and night time data for geothermal and mineral mapping in Eastern Africa.

To extract meaningful information from the ASTER data, several spectral processing techniques have been developed and tested. For instance, Oskouei & Nouri, 2011 used band ratios for detection of geothermal resources using ASTER data in Sabalan, Iran. Similarly, Ghosh et al, 2016, used band ratio to delineate alteration and related clay minerals in Sakoli Belt Mahasrashatra in India. Fakhari et al, 2019 used color composite technique to delineate hydrothermal alteration zone for porphyry system in Jebal-Barez area SE Iran. Banerjee et al, 2019, used Relative Band Depth (RBD) to identify hydrothermal alteration zone in Singhbhum Shear zone in India using Landsat 8 OLI data. Other spectral processing technique include logical operator algorithms as demonstrated by Mars & Rowan, 2006 by carrying out regional mapping of phyllic and argillic alterations in the Zagro Magmatic arc, Iran.

This paper aims to identify hydrothermal alteration minerals in the study area using spectral processing techniques such as color composite, band ratios, relative band depth and logical operator algorithms on ASTER data. The study is aimed to prove capability of ASTER sensor in mapping and delineating hydrothermal alteration minerals and zones.

2. AREA OF STUDY AND THE GEOLOGICAL SETTING

Olkaria and Eburru geothermal systems are within the central sector of the Kenyan Rift valley and are in Nakuru county Kenya. The central sector of the Kenya rift is flanked by plateau composed of Precambrian rocks and are extensively covered by rift lavas and pyroclastics of the late Cenozoic age (Baker et al, 1988). The region is associated with quaternary volcanism. Numerous studies have been done in order to understand the evolution of the Kenyan rift. For instance, Clarke, Woodhall, 1990, indicated that the tectonic and volcanic regimes which have formed the Kenyan rift commenced in the early to mid-Miocene. Conti et al., 2021, pointed out that, the western rift shoulder i.e. Mau escarpment is bordered by the Mau fault. This fault system is later overprinted by younger faults and partially covered by younger deposits. Then inner trough which host Lake Nakuru and Lake Naivasha is bordered by the Mau fault to the west and the Bahati and Kinangop fault to the east in the lower most portion of the rift valley.

The volcanic and structural development of the Kenya rift has been studied for many years using chronological and litho-stratigraphic correlation methods (Omenda, 1998). It is generally agreed that the tectonic and volcanic regimes which have formed the Kenya rift commenced in the early to mid-Miocene, approximately 25-30ma (Clarke, Woodhall, 1990). As highlighted by Omenda, 1998, the rift related activities started during the early miocene, with extensive basltic and phonolitic volcanism on the crest of an uplifted dome. The early volcanic rocks crop out in the northern part of the rift and on the eastern shoulder. They overlie the late Proterozoic schists and gneisses of the Mozambique mobile belt that occur at depth greater that 5km. The oldest volcanic rocks in the area are the lower Miocene basalts inked with sub-aerial fissure and flood style volcanism (Smith & Mosley, 1993).

The study areas are located within the Nakuru county on the flooer of Central Kenyan rift. According to Conti et al., 2021, the rift is in an advanced stage of rifting process with magmatism and tectonic events currently located in the trough of the main rift. Figure 2 below shows the geological map of the study area but showing other areas on the rift floor.

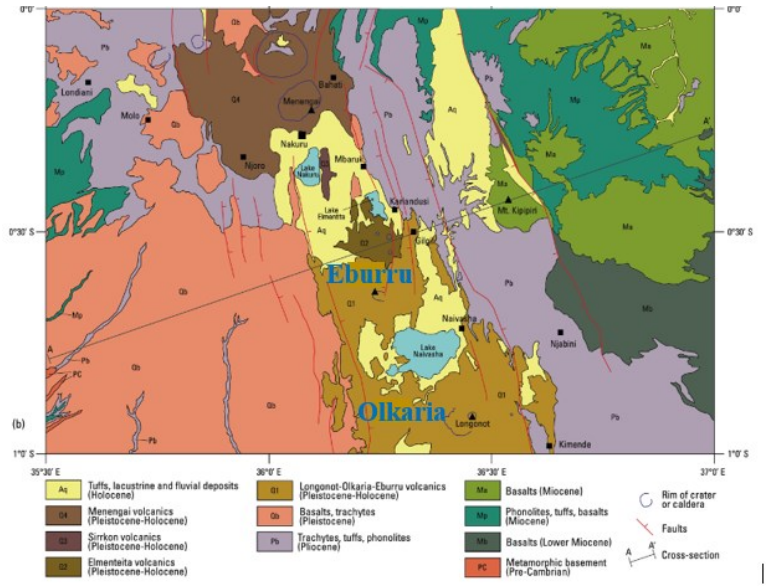

Figure 2: Geological map of the study area (Conti et al., 2021)

2. DATA SET AND METHODOLOY

2.1 ASTER Data

Two scenes of daytime ASTER surface reflectance VNIR and Crosstalk corrected SWIR (AST_07XT) acquired on 15th October 2004 was used for this study. This data was retrieved from **https://search.earthdata.nasa.gov/search** was corrected for both atmospheric and viewing geometry effects. To minimize interference of the reflected light between SWIR arrays detectors, crosstalk corrected surface reflectance was chosen. The data contain measures of the fraction of the incoming solar radiation reflected from the earth surface to the ASTER instrument. The scenes were chosen on a cloud-free day and was already georeferenced to the UTM zone 37 S projection using the WGS-84 datum.

2.2 Methodology

The data was first pre-processed by layer stacking of VNIR & SWIR resulting into a 9 band image data and then resizing (spatial subset) to the area of interest. This was important because it allows multiple combination of bands from different wavelength range thus allowing in-depth qualitative analysis and quick detection of alteration minerals.

2.2.1 Color composite

Color composite images were used to acquire general information about the land cover and lithology in the study area. Red, Green, Blue (RGB): 3-2-1, 6-3-1 and 4-6-8 were used for this study. They were used as a rough guide to detect main lithological and alteration differences together with delineating highly vegetated areas.

2.2.2 Normalized Difference Vegetation Index (NDVI) calculation

NDVI is a simple numerical indicator that can be used to measure vegetation cover change. It is calculated by the equation.

$$NDVI = \frac{NIR - RED}{NIR + RED}$$

Where NIR and RED stand for the reflectance values in the near infrared and visible red spectral regions respectively (Bolanio et al, 2015). The result is a ratio with possible values between -1 and +1. Values above 0 are generally considered vegetated with higher values indicating denser vegetations. For this study, NDVI map was created using band 2&3 using EVNI/Transform/NDVI. Threshold used for non-vegetated areas was between 0-0.4 while those with value <0 were pixel under water and had no data.

2.2.3 Logical Operator Algorithms

This was aimed at mapping hydrothermally altered Al-OH spectral absorption features associated with alunite, kaolinite and sericite-muscovite. As suggested by Mars, (2013), this was filtered using logical operators ((float(b3)/b2) le 1.35) and (b4 gt 260) and ((float(b4)/b5) gt 1.25) and ((float(b5)/b6) le 1.05) and ((float(b7)/b6) ge 1.03).

2.2.4 Band ratio

It is a technique where the procedure involves the division of two bands, where the bands with high reflectance features of a given material is assigned numerator while the absorption features for the same material is assigned the denominator (Rouskov et al, 2014). The technique improves the contrast and enhances compositional information by highlighting spectral differences between bands and the reduction of the topographic effects. For this study, band ratio 4/6 was used as an indicator for hydrothermal alterations. Clay minerals show high reflectance in band 4 and low reflectance in band 6.

2.2.5 Relative Absorption Band Depth (RBD)

In this case, a band depth image is created by dividing the sum of the two highest reflectance spectral bands which may be in a sequence in reflectance channel or not by the lowest absorption features. The resultant product is a one band image with pixel values which are proportional to the depth of the absorption feature at the wavelength of the reflectance minimum. The Relative Band Depth (RBD) detects the clay bearing groups of minerals based on the location and depth of the absorption's features. In this study, band depth (b4+b6)/b5 was used to highlight kaolinite/alunite, (b5+b7)/b6 was used to highlight sericite/illite/muscovite and (b7+b9)/b8 to map calcite/epidote/calcite.

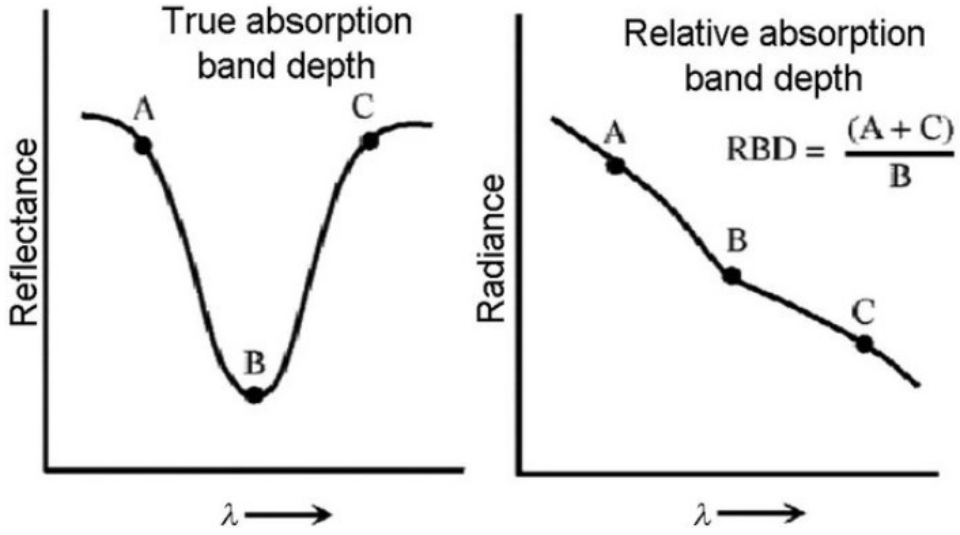

Figure 3:True and relative absorption band depths (Banerjee et al, 2019)

3. RESULTS AND DISCUSSION

3.1 Color composite images: ASTER band combinations in RGB (red, green, blue)

RGB composite image for band 3-2-1 has been prepared for the study area (Figure 4a). The red color clearly shows mapped areas which are highly vegetated. On the other hand, color composite image for band 4-6-8 composite images (Figure 4b) was typically used to show argillic and phyllic alteration. The result shows slight discrimination with the argillic and phyllic altered rocks in amethystine tones.

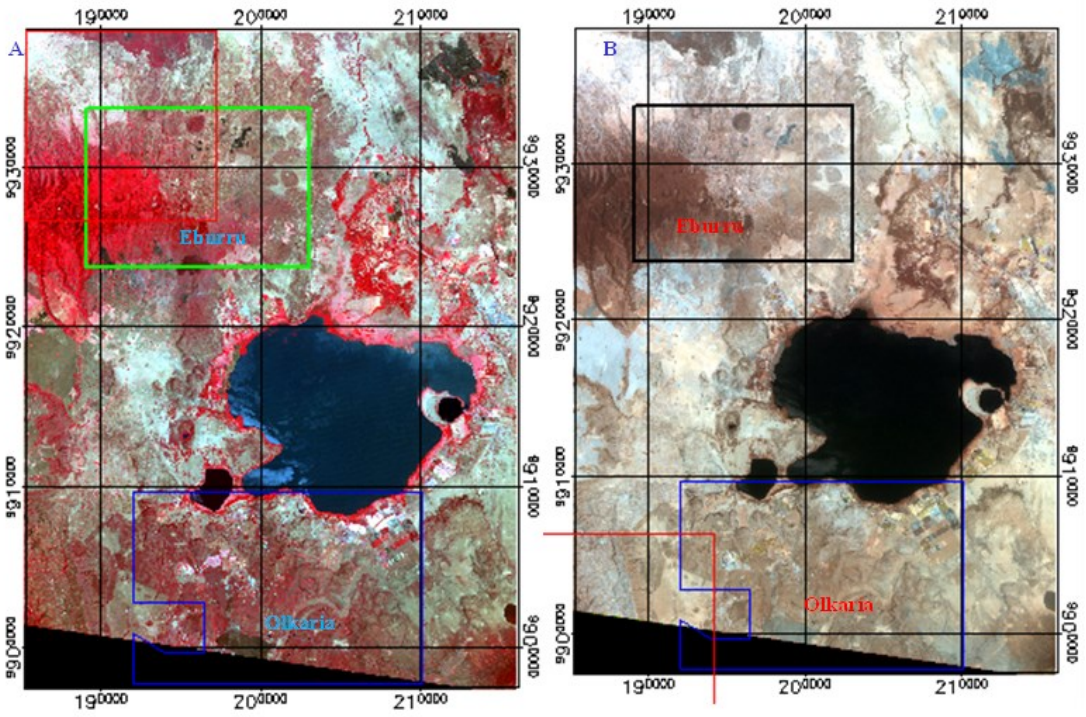

Figure 4: Color composite images for (A) band 3-2-1 and (B) band 4-6-8

3.2 Normalized Difference Vegetation Index (NDVI) map

The map was prepared using band 2&3 using ENVI/ Transform/NDVI algorithm (Figure 5a). The vegetated areas are represented by red areas. Thresholds between 0-0.4 were used to map vegetated areas while <0 pixels under water had no data.

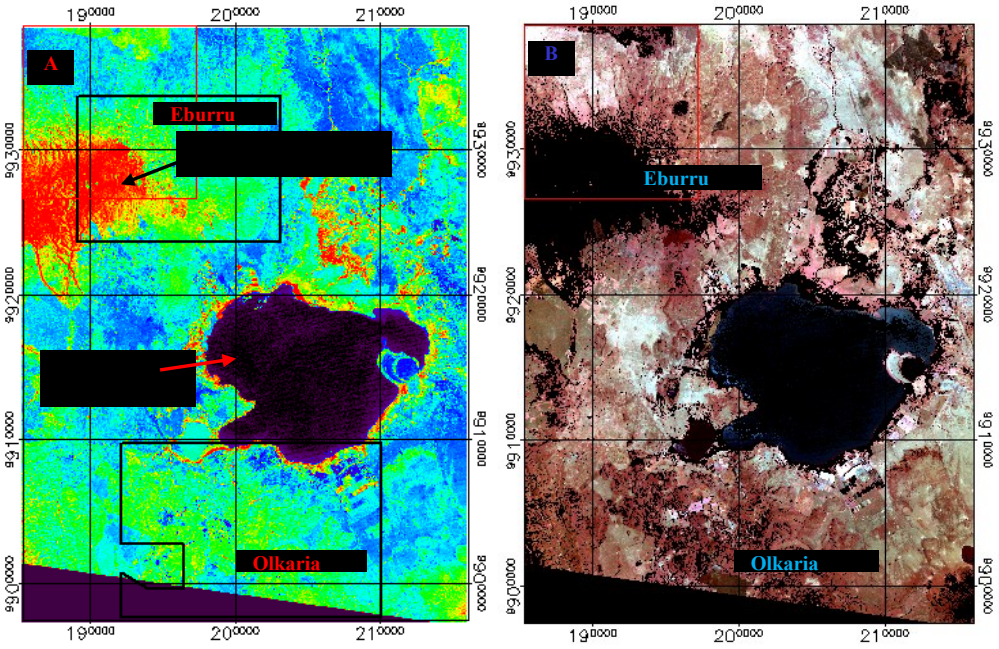

Figure 5: NDVI map(A) and (B) map showing masked vegetation and water pixels

3.3 Logical Operator Algorithm

This technique managed to map pixels of phyllic and argillic hydrothermal alteration mineral whose deepest absorption features occurs approximately at 2.16µm. From the result, very few pixels were mapped as argillic altered areas (Figure 6).

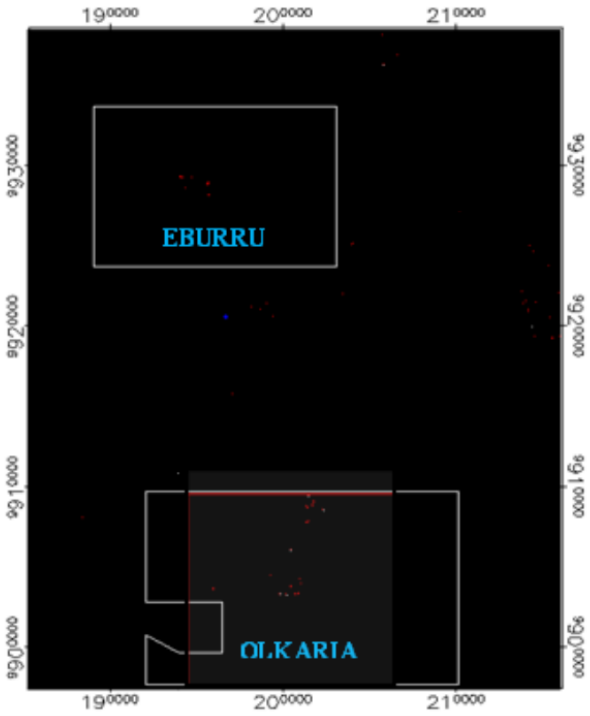

Figure 6: Red pixels shows area with argillic/ phyllic alteration

3.4 Band ratio

Figure 7a shows SWIR band ratio 4/6. It was found to be a good indicator of hydrothermal alteration minerals. Characteristically, clay minerals show high reflectance in band 4 and low reflectance in band 6. A threshold of between 1.5-2.3 was used to extract yellow-colored pixels which are indicator of alteration zones. The result is consistent with RGB 4-6-8 color composite image showing altered rocks in amethystine tones (figure 7b).

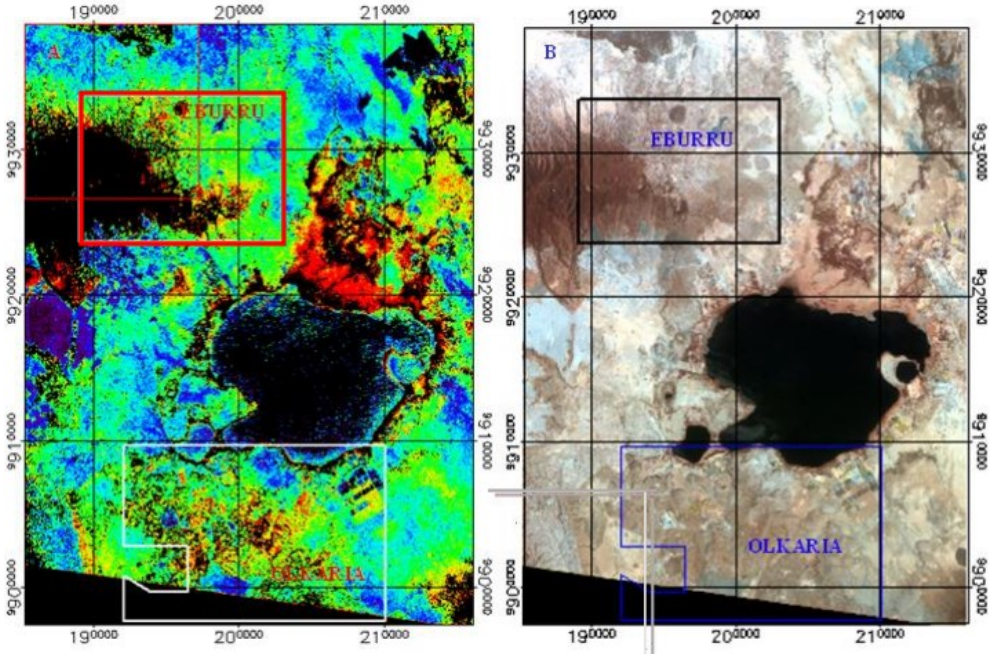

Figure 7: B4/B6 alteration image (A) compared with color composite image for band 4-6-8

3.5 Relative Band Depth

The RBD detects clay bearing group of minerals based on the location and depth of the absorption features. RBD images sensitive to kaolinite/ alunite, sericite/illite/ muscovite and calcite/epidote /chlorite was used to identify them in the study area. Results shows the most dominant alteration minerals are either alunite/ kaolinite (Figure 8a). Very few pixels were mapped indicating presence of illite/muscovite in the study area (Figure 8b). However, zones of alteration associated with either calcite/epidote/ chlorite were identified in Olkaria central region (Figure 8c). In addition, a Relative Band Depth of argillic, phyllic and propylitic alterations in RGB image was generated. In this case: Red= kaolinite/alunite group (b4+b6)/b5, Green = illite group (b5+b7)/b6, Blue = chlorite group (b7+b9)/b8 (Figure 8d). Magenta color shows high values in red and blue band which indicate a mixture of kaolinite and chlorite group of minerals. Green area shows phyllic alteration associated with illite, sericite and muscovite and lastly, cyan color indicates high values in green and blue bands. However, this is interpreted as an anomaly since the pixels falls on water area of L. Naivasha

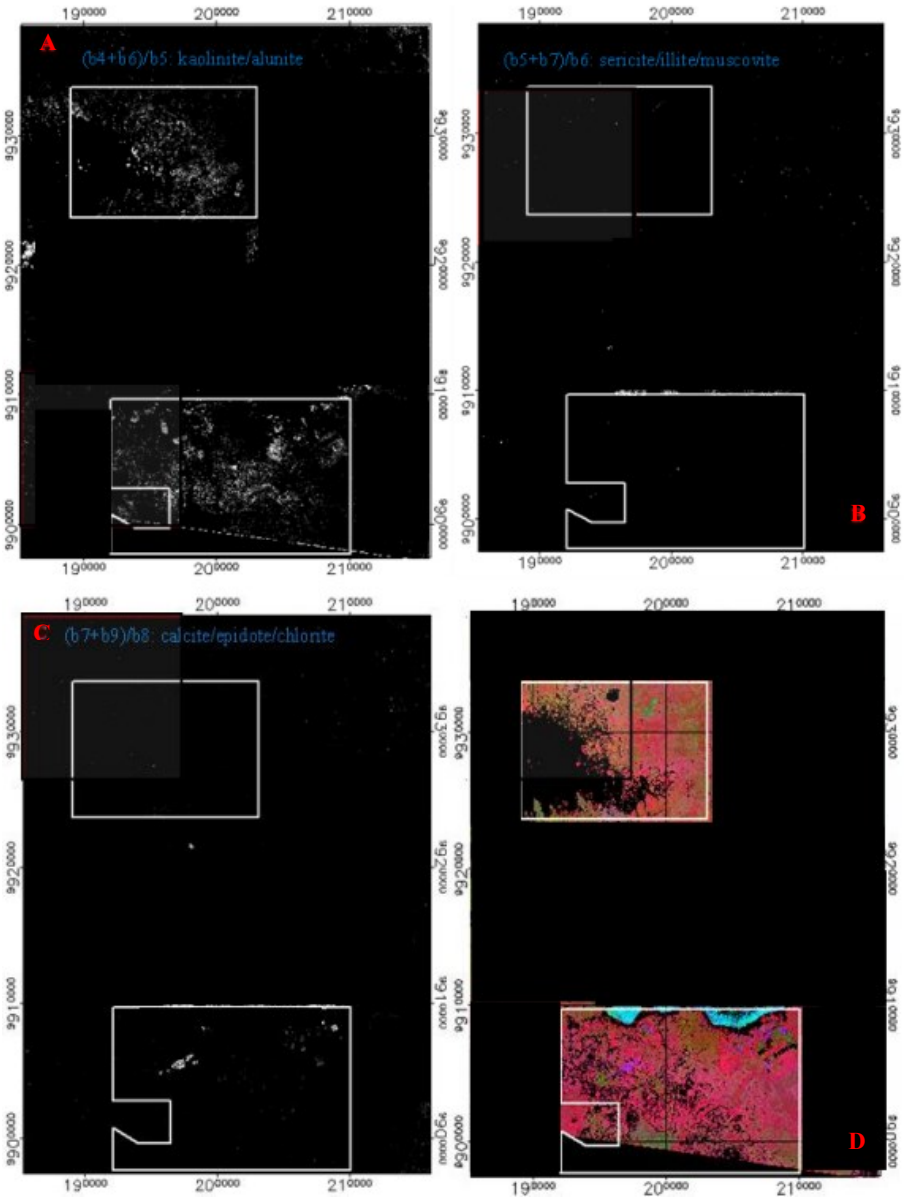

Figure 8: RBD for mapping kaolinite/alunite (B) for mapping sericite/illite/muscovite(C) for mapping calcite/ epidote/chlorite(D) RGB images from the three RBD depths

4. CONCLUSION

This study proved capability of ASTER sensor to identify and delineate alteration minerals and mineral assemblages. Results derived from this study confirm ASTER data can be used as tool for initial steps of geothermal exploration. High accuracy maps derived from the processed images can allow delineation of alteration zones of potential geothermal resource thus reducing time and cost required for field exploration and evaluation procedure

5. RECOMMENDATION

Fieldwork is highly recommended to validate the results derived from the study. Future study to include TIR bands to assess surface temperature anomalies in the study area.

Acknowledgement

I appreciate the Land Processes Distributed Active Archive Centre (LPDAAC) for providing free access to data used for this study.

REFERENCES

Abrams, M., & Yamaguchi, Y. (2019). Twenty years of ASTER contributions to lithologic mapping and mineral exploration. *Remote Sensing*, *11*(11), 1–28. https://doi.org/10.3390/rs11111394

Abubakar, A. J., Hashim, M., & Pour, A. B. (2019). Identification of hydrothermal alteration minerals associated with geothermal system using ASTER and Hyperion satellite data: a case study from Yankari Park, NE Nigeria. *Geocarto International*, *34*(6), 597–625. https://doi.org/10.1080/10106049.2017.1421716

Alimohammadi, M., Alirezaei, S., & Kontak, D. J. (2015). Application of ASTER data for exploration of porphyry copper deposits: A case study of Daraloo – Sarmeshk area , southern part of the Kerman. *Ore Geology Reviews*, *70*, 290–304. https://doi.org/10.1016/j.oregeorev.2015.04.010

Baker, B. H., Mitchell, J. G., & Williams, L. A. J. (1988). Stratigraphy, geochronology and volcano-tectonic evolution of the Kedong–Naivasha–Kinangop region, Gregory Rift Valley, Kenya. *Journal of the Geological Society*, *145*(1), 107–116. https://doi.org/10.1144/gsjgs.145.1.0107

Banerjee, K., Jain, M. K., Jeyaseelan, A. T., & Panda, S. (2019). Landsat 8 OLI data for identification of hydrothermal alteration zone in Singhbhum Shear Zone using successive band depth difference technique - A new image processing approach. *Current Science*, *116*(10), 1639–1647. https://doi.org/10.18520/cs/v116/i10/1639-1647

Bolanio, K. P., Santillan, M. M., Santillan, J. R., & Daguil, R. C. (2015). Using normalized difference vegetation index (NDVI) to assess vegetation cover change in mining areas of tubay Agusan del norte. *ACRS 2015 - 36th Asian Conference on Remote Sensing: Fostering Resilient Growth in Asia, Proceedings*, (October).

Clarke, Woodhall, A. & D. (1990). *Geological, volcanological and hydrogeological controls on the occurrence of geothermal activity sorrounding Lake Naivasha, Kenya*. Nairobi.

Conti, P., Pistis, M., Bernardinetti, S., Barbagli, A., Zirulia, A., Serri, L., … Ghiglieri, G. (2021). Tectonic setting of the kenya rift in the nakuru area, based on geophysical prospecting. *Geosciences (Switzerland)*, *11*(2), 1–23. https://doi.org/10.3390/geosciences11020080

Elsaid, M., Aboelkhair, H., Dardier, A., Hermas, E., & Minoru, U. (2014). Processing of Multispectral ASTER Data for Mapping Alteration Minerals Zones: As an Aid for Uranium Exploration in Elmissikat-Eleridiya Granites, Central Eastern Desert, Egypt. *The Open Geology Journal*, *8*(1), 69–83. https://doi.org/10.2174/1874262901408010069

Fakhari, S., Jafarirad, A., Afzal, P., & Lotfi, M. (2019). Delineation of hydrothermal alteration zones for porphyry systems utilizing ASTER data in Jebal-Barez area, SE Iran. *Iranian Journal of Earth Sciences*, *11*(1), 80–92.

Fatima, K., Khan Khattak, M. U., Kausar, A. B., Toqeer, M., Haider, N., & Rehman, A. U. (2017). Minerals identification and mapping using ASTER satellite image. *Journal of Applied Remote Sensing*, *11*(04), 1. https://doi.org/10.1117/1.jrs.11.046006

Ghosh, U. K., Kesari, M. P., & Naik, K. K. (2016). Digital image processing of multispectral ASTER imagery for delineation of alteration and related clay minerals in Sausar Belt-a case study. *Indian Journal of Geosciences*, *70*(1), 49–58.

Hewson, R., Mshiu, E., Hecker, C., van der Werff, H., van Ruitenbeek, F., Alkema, D., & van der Meer, F. (2019). The application of day and night time ASTER satellite imagery for geothermal and mineral mapping in East Africa. *International Journal of Applied Earth Observation and Geoinformation*, (October), 101991. https://doi.org/10.1016/j.jag.2019.101991

Mars, J. (2013). Hydrothemal Alteration Maps of the Central and Southern Basin and Range Province of the United States Compiled from Advnaced Spaceborne Thermal Emission and Reflection Radiometer(ASTER) Data.pdf. Retrieved from https://pubs.usgs.gov/of/2013/1139/of2013-1139.pdf

Mars, J. C., & Rowan, L. C. (2006). Regional mapping of phyllic- and argillic-altered rocks in the zagros magmatic arc, Iran, using advanced spaceborne thermal emission and reflection radiometer (ASTER) data and logical operator algorithms. *Geosphere*, *2*(3), 161–186. https://doi.org/10.1130/GES00044.1

Omenda, P. A. (1998). The geology and structural controls of the Olkaria geothermal system, Kenya. *Geothermics*, *27*(1), 55–74. https://doi.org/10.1016/S0375-6505(97)00028-X

Oskouei, M. M., & Nouri, T. (2011). Band ratio method for detection of geothermal sources using aster data , (January).

Pour, Amin Beiranvand, & Hashim, M. (2012). The application of ASTER remote sensing data to porphyry copper and epithermal gold deposits. *Ore Geology Reviews*, *44*, 1–9. https://doi.org/10.1016/j.oregeorev.2011.09.009

Pour, Amin Beiranvnd, Hashim, M., & Marghany, M. (2011). Using spectral mapping techniques on short wave infrared bands of ASTER remote sensing data for alteration mineral mapping in SE Iran, *6*(4), 917–929. https://doi.org/10.5897/IJPS10.510

Rouskov, K., Popov, K., & Stoykov, S. (2014). Some Applications of the Remote sensing in Geology by using ASTER Images. *Researchgate*, (January 2014).

Rowan, L., Hook, S., Abrams, M., & Mars, J. (2003). Mapping Hydrothermally Altered Rocks at Cuprite, Nevada, Using the Advanced Spaceborne Thermal Emission and Reflection Radiometer (ASTER), a New Satellite-Imaging System. *Economic Geology*, *98*,

1019–1027. https://doi.org/10.2113/gsecongeo.98.5.1019

Smith, M., & Mosley, P. (1993). Crustal heterogeneity and basement influence on the development of the Kenya Rift, East Africa. *Tectonics*, *12*(2), 591–606. https://doi.org/10.1029/92TC01710

Testa, F. J., Villanueva, C., Cooke, D. R., & Zhang, L. (2018). Lithological and hydrothermal alteration mapping of epithermal, porphyry and tourmaline breccia districts in the argentine andes using ASTER imagery. *Remote Sensing*, *10*(2), 1–45. https://doi.org/10.3390/rs10020203